Article:
Deng, F., Jiao, Z., Liang, B. et al. (2 more authors) (2017) Spike Effects on Drag Reduction for Hypersonic Lifting Body. Journal of Spacecraft and Rockets, 54 (6). pp. 1185-1195. ISSN 0022-4650

https://doi.org/10.2514/1.A33865

Spike Effects on Drag Reduction for Hypersonic Lifting-body

Fan Deng[1], Zihan Jiao[4] and Bingbing Liang[5]
Science and Technology on Space Physics Laboratory, China Academy of Launch Vehicle Technology, Beijing, China

Feng Xie[2] and Ning Qin[3]
Department of Mechanical Engineering, University of Sheffield, Sheffield, UK

High lift-to-drag ratio is considered crucial for high altitude and long endurance hypersonic vehicles. One of the simplest and most useful methods is to install an aerospike in front of the vehicle's nose. In this paper, the flight aerodynamic characteristics are investigated by simulating and comparing the lifting-body with or without the aerospikes at Ma=8. The flow fields around aerospikes using different spike lengths and a hemispherical disk along with the lifting-body are analysed. The results of aerodynamic characteristics indicate that L/D=2 is the best ratio of spike length to nose diameter. By comparing with the baseline model, maximum drag reduction of the nose's part is 49.3% at α=8º using hemispherical disk. In addition, three shapes of aerospike disks are compared to search for a best disk for hypersonic drag reduction. The best drag reduction is found for the double flat faced disk aerospike, which gives a pressure drag reduction of 60.5% of nose's part at α=8º. Furthermore, when the flight angle of attack increases, the drag increases significantly. Employing certain installation angle is shown to effectively improve the drag reduction around the angle of attack and results in improving the lift-to-drag ratio. At the

[1]Senior Engineer, Aircraft design group, dengfan8245@sina.cn.

[2]PhD, Department of Mechanical Engineering, fxie2@sheffield.ac.uk.

[3]Professor, Department of Mechanical Engineering, Associate fellow of AIAA, n.qin@sheffield.ac.uk.

[4]Engineer, Aircraft design group, zihan325@hotmail.com.

[5]Senior Engineer, Aircraft design group, sherrylovely@gmail.com.

end, the lift-to-drag ratio of the final optimized design is 9.1% better than that of the baseline model. The pressure centre is moved forward by 1.6%, barely influencing the vertical static-stability of the vehicle.

Nomenclature

L	= aerospike length, mm
l_1	= the length between the second disk and vehicle's nose, mm
D	= vehicle nose diameter, mm
L_v	= vehicle length, mm
L_1	= first cone length, mm
L_2	= second cone length, mm
Φ_1	= first cone base diameter, mm
Φ_2	= second cone base diameter, mm
S	= span of the triangular wings, mm
χ	= leading edge swept angle of the wing, °
θ	= angle between windward reattachment point and the horizontal axis, °
P	= static pressure, Pa
P_∞	= inflow static pressure, Pa
Ma	= Mach number
Re	= Reynolds number based on the vehicle length
α	= angle of attack, °
α_s	= aerospike installation angle, °

C_D = drag force coefficient

C_L = lift force coefficient

k = lift-to-drag ratio

Xcp = pressure center coefficient

I. Introduction

Reduction of heat load and drag are two important aspects throughout the design process for hypersonic vehicles. To reduce the heat load, imposing bluntness at the nose of the hypersonic vehicles is a common and effective way. However, the forced bluntness dramatically increases the wave drag of the vehicles. On the other hand, some techniques of wave drag reduction are devised, including a counter flowing jet [1], energy deposition [2] and aerospikes. The former two methods require jet flow generators or external energy sources. By contrast, the aerospike is the simplest and most feasible structure to reduce the wave drag for hypersonic vehicles and takes up a small space of the vehicles.

By means of transforming the strong bow shock into weaker and conical oblique shock waves, and creating a separated flow region, the aerospike shields the blunt-body from the incoming flow. Thus, a low pressure and low temperature recirculation region or separation bubble are created near the stagnation region. The low pressure gives low wave drag of vehicles. Drag reduction for a blunt cone model using the aerospike has been a research topic for half a century. Numerical and experimental investigations have been carried out for a variety of objectives. Different lengths and geometries of aerospikes, Reynolds number, Mach number and test configurations have been considered as typical parameters during these studies [3, 4].

Most of the investigations conducted for spiked blunt bodies have concluded that the use of aerospikes can drastically reduce the aerodynamic drag at hypersonic speeds, for certain ratios of the

spike length to the diameter of the body. Crawford [5] conducted an extensive experimental investigation of drag and aerodynamic heating on hemisphere cylindrical model with pointed spikes of different L/D ratios at Mach 6.8. Motoyama et al. [6] measured the variation of drag and pitching moment coefficients with incidence angles (up to 8º) of a spiked hemisphere cylindrical model at Mach 7. They also experimentally investigated the aerodynamic and heat transfer characteristics of conical, hemispheric, flat-faced aerospike for L/D=0.5, 1.0. The disk aerospike (L/D=1.0 and disk diameter 10mm) showed more effective in drag reduction and less heating. Mehta [7] numerically studied hemispheric, flat faced and conical disk spikes for L/D 0.5, 1.5,2.0 at $\alpha=0^{\circ}$ for Mach number 6. Menezes [8,9] studied hemispheric disk, flat and pointed plain spike, discussed the variation of surface pressure and heat flux with spike length and the impact of angle of attack on the total drag. And Kulkarni [10] extended the speed region to Mach 8 on the same model at zero incidence. Gauer and Paull [11] researched on a blunt conical shape of spike which had a variable length (L/D varied from 1 to 4) at Mach 5~10. The performance of spikes at an incidence in very low Reynolds number environments was investigated by Sims et al. [12]. The models were equipped with a pointed spike of variable length (L/D up to 5).

Studies conducted by Kalimuthu et al. [13] at Mach 6 showed that the effectiveness of the aerospikes can be increased further by the use of flat faced or hemispheric faced spike disks. Asif [14] numerically studied a standard blunt nose body with pointed aerospikes, and discovered the aerospikes reduce the aerodynamic drag in supersonic flow, also causes an increase in the normal force, but resulting in an adverse effect on the static stability at the same time. Gerdroodbary [15] numerically studied effectiveness of disk/aerospike assemblies as retractable drag- reduction devices for large-angle blunt cones flying at various angles of attack at Mach 5.75. Elsamanoudy [16] designed a reattachment ring

for spiked hemispheric bodies. Numerical results showed the reattachment ring and the spike-disk-spike assembly add up synergistically to achieve a maximum drag reduction of 69.82% in hypersonic flow. Tahani [17] numerically studied flat and hemispheric disk for hemispheric body and showed that the designs produced 60 % reduction in drag.

Disk configurations with two hemispheric caps of various sizes have also been investigated for the effect on the aerodynamic drag of a hemisphere cylinder. Yadav and Guven [18] did a recent investigation for heat transfer rates and aerodynamic drag of a hemispheric cylinder with double disk aerospike at Mach 6.2. The peak reattachment pressure on the main body is reduced by 50% of the base body stagnation pressure and drag reduction is observed 47% for all disk aerospike. Joshi [19] numerically studied single and double disk aerospikes with different L/D ratios and disk radius. The results demonstrated double disks aerospike with L/D=2.0 produced 74.7% drag reduction, whereas the single disk produced 70% reduction in drag. Ahmed and Qin [20, 21] conducted a bi-objective (aerodynamic drag and heating) design optimization by parameterizing the spike length, the disk shape and the blunt nose shape. The design of hypersonic spiked blunt bodies was optimized using the multi-objective NSGA-II algorithm coupled with kriging surrogates at Mach 6.

Srulijes [22] studied the flow field around three-dimensional blunt bodies equipped with forward facing aerospikes for a large range of angles of attack at Mach 4.5, found the drag on all spiked bodies increases at higher angles of attack. To solve this problem, Schulein [23,24] introduced the concept of “pivoting spike” in which the aerospike is maintained aligned with the freestream direction while the whole body is at different incidences. He experimentally examined the pivoting spike in Mach 2, 3, and 5 with up to 30º incidence. The results presented clearly the advantages of the aligned aerospikes over the conventional fixed aerospikes.

In order to explore the application of aerospike on aircrafts, McWherter [25] analyzed the aerodynamic, structural, and mechanical proof-of-concept of a large multi-stage telescoping nose aerospike installed on F-15B airplane. He assessed the effect of the aerospike on the stability, controllability, and handling qualities of the airplane up to Mach 1.8. Khurana [26] studied a simple lifting-body configuration deduced from the X-33 fuselage with different aerospikes at Mach 7 in a wind tunnel. The experimental results showed a large increase in the lift-to-drag ratio and a marginal increase in pitching moment compared to non-aerospike case, indicating the practical feasibility for eventual future applications to spacecraft.

This paper presents an investigation on spike drag reduction effects on a double-cone-wing lifting-body vehicle at hypersonic speed. The influence of different spikes on the overall performance of the whole configuration is analyzed along with the effect on the pressure center of lifting-body vehicle. The study covers the effects of spike length, three different spike designs, and the spike installation angle at the cruise condition. This is the first time that a pivoting spike has been investigation on a lift-body-wing configuration at hypersonic speeds. The research leads to a suitable aerospike design for the cruise flight angle of attack to achieve the maximum drag reduction. The behavior of the spike at off-design condition is also analyzed for a range of incidences.

II. Problem Definition and Solution Approach

In this paper, a hypersonic vehicle flying at a Mach 8 and an altitude of 40 km in a standard atmosphere is investigated. Flow over the vehicle with a hemispheric disk aerospike is simulated numerically at different length to diameter ratios. The hemispheric disk aerospike as well as a flat conical disk aerospike are comparatively studied for L/D ratio of 2.0 to understand the flow field features and mechanisms of drag reduction. Both double-disk aerospikes with and without an

installation angle are employed for enhancing the drag reduction effect at moderate angles of attack.

2.1 Lifting-body geometry and aerospike configurations and flow conditions

The research of this paper is based on a general spiked hypersonic vehicle with both a main body and an aerospike. The part of main body can be divided into a double-cone and two triangular wings as shown in Fig. 1. The overall length of the double-cone is 3,000mm. The first cone has a base diameter of 300mm and length of 700mm, meanwhile, the second cone has a base diameter of 450mm and length of 2,300mm. The span of the triangular wings is 1,500mm with the same length as the second cone and the leading edge swept angle of the wing is 75.6°. The part of aerospike consists of a long cylindrical spike and a disk, which is shown in Fig. 2. To investigate the influence of the spikes lengths, the diameter of spike is fixed to be 0.1D and compared different lengths of spikes, including L/D = 1.0, 1.5, 2.0, 2.5, 3.0. (D is the nose diameter of 100mm.) The shapes of disks are hemispherical, single flat faced and double flat faced. To simplify the names of the shapes cited above, single flat faced disk is named SFF and double flat faced disk is simplified to be DFF. The radius of the front disk is fixed to be 0.15D. In addition, for DFF the radius of the second disk is 0.4D and the disk is 1.3D away from the vehicle nose.

The incoming flow conditions of all simulations are static pressure of 287Pa, static temperature of 250K and freestream Mach number of 8. Accordingly, the Reynolds number is $Re=1.897x10^6$. At this Reynolds number, the flow can be assumed as laminar flow [27, 28]. Thus, the simulations are all in laminar.

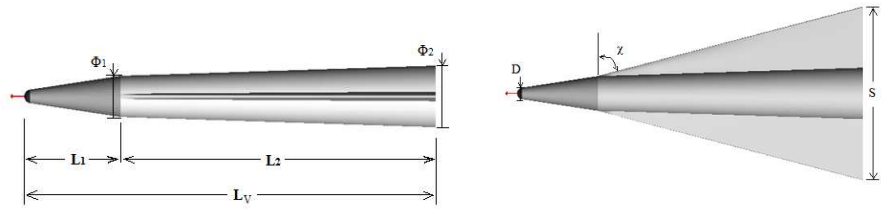

Fig. 1 Lifting-body vehicle with a aerospike.

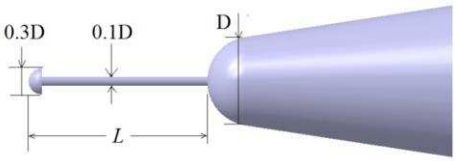

(a) Hemispheric disk aerospike, L/D=1.0,1.5,2.0,2.5,3.0

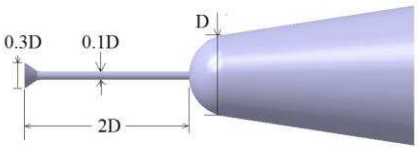

(b) Single Flat Faced disk aerospike model (SFF)

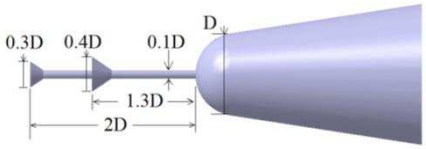

(c) Double Flat Faced disk aerospike model (DFF)

Fig. 2 Enlarged views of aerospikes near the nose of the lifting body (Fig.1).

2.2 Computational Grids

To simulate the flow fields, a half body mesh is generated by Gridgen because all the geometries are symmetric without a yaw angle. In Fig. 3, the generation of mesh has been shown in details. All the meshes are multi-block-structured mesh and the mesh size varies from 6.0 to 9.5 million. Most of the nodes are clustering near the nose and the spike to capture the details of flow structures. The height of first cell from the wall is 0.5×10^{-3}m to resolve the boundary layer shear near the wall.

There are three kinds of boundary conditions in the simulations, including adiabatic wall, pressure farfield and pressure outlet. The aerodynamic coefficients are obtained by the reference length of 3m and reference area of 0.2m^2 which are based on the length of main body and the area of the second cone base, respectively. The reference point of pressure center is set at the center vertex of the vehicle nose.

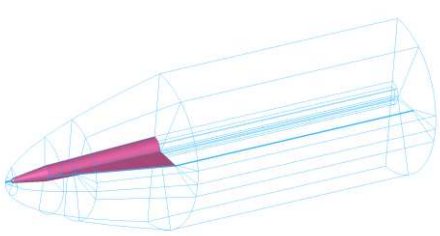

(a) Topoligy of mesh

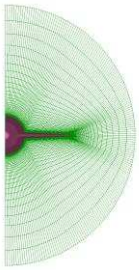

(b) Outflow-boundary mesh

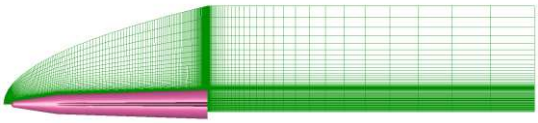

(c) Symmetry-boundary mesh

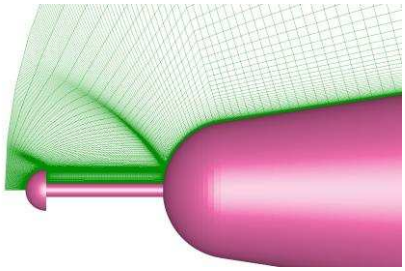

(d) Symetry-boundary mesh near the nose

Fig. 3 Introduction of mesh.

2.3 Numerical methods

A finite volume method solver in Ansys, a commercial CFD package, is used to simulate the flow field, solving compressible N-S equations. In the simulations, a second order discretization is used and the Roe scheme (an approximate Riemann solver) is also employed in order to calculate the numerical fluxes for shock capturing. All cases are using density-based and steady-time-independent settings. The time steps are based on Courant-Friedrichs-Lewy number (CFL) and under-relaxation factors. The CFL number is set from 0.01 to 0.3 during the first 500 iterations and is kept 0.3 to the end of simulations to ensure the calculation process does not diverge at the initial steps and has a relatively fast convergence afterwards. After the residuals of the simulations is reduced by 5 orders and the total drag is steady, the simulation is considered to be convergent.

To validate the numerical solver, an experimental case by Kalimuthu R [13] is compared. The experimental model has a blunt body installed with a hemispherical aerospike at the nose. The diameter of the hemispheric disk was 0.1D, the length of the spike was 2D (see model details in ref [13]). In that

case, the incoming flow conditions were freestream Mach number of 6, stagnation pressure of 830,000Pa and stagnation temperature of 450K. The reference length was based on the diameter of the nose, as well as, the reference area was based on the base area of the blunt body. The drag coefficients were obtained at different angles of attack, from 0°~8°. Fig. 4(a) shows the comparison of drag coefficients at different angles of attack. Comparing the simulation outcomes with the experimental results, the error turns out to be less than 4.2%. In addition, a density gradient contour of the simulation is compared with the Schlieren photograph of the experiment in Fig. 4(b). The foreshock, recirculation region and shear layer are captured around the model. Based on the preceding expression, the validation proves that the settings of the simulations are satisfied to investigate the performance of aerospikes.

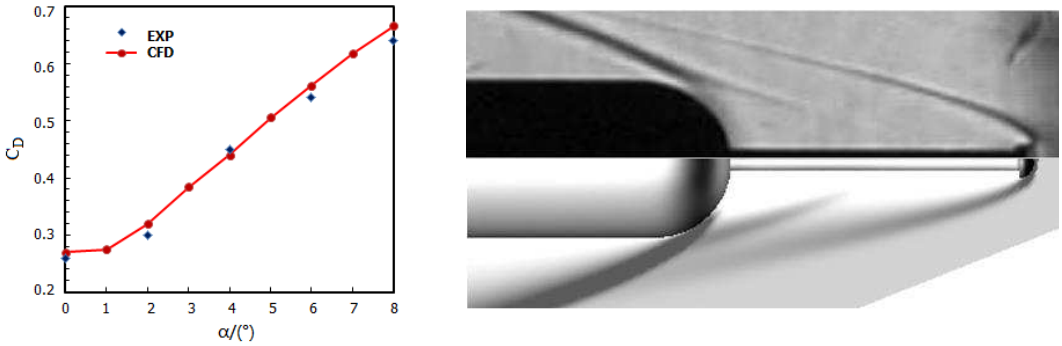

(a) The comparison of drag coefficients between simulations and experiments

(b) The comparison of density gradient contour (bottom) and the Schlieren photograph of the experiment (top)

Fig. 4 Simulation validation.

III. Results and Discussion

3.1 Effects of L/D ratio on drag

By separately integrating the pressure of different parts, each parts' values of pressure drag are obtained. Meanwhile, the viscous drag is considered as a whole value because this research focuses on

the reduction of pressure drag. Fig. 5 shows the percentages of the pressure drag of each component of the vehicle and the total viscous drag. Note that the largest drag comes from the pressure drag of the vehicle nose, taking 33% of the total drag (shown in Fig. 5). The total drag of the whole vehicle can be reduced effectively through the nose's pressure drag reduction by the aerospike.

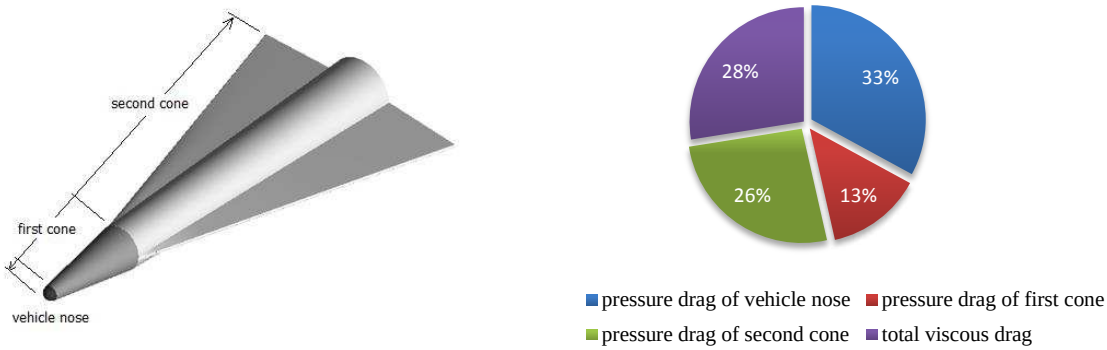

Fig. 5 Drag distribution map of vehicle components.

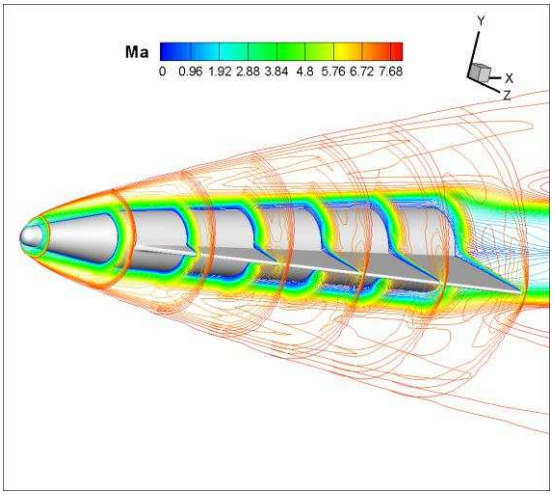

Fig. 6 A typical flow field for lifting-body.

The investigation of the L/D influence is conducted on a model with a hemispheric disk aerospike. The spike length varies from 1D to 3D with a step 0.5. A total of 5 models (including the baseline model) are investigated. Meanwhile, Fig. 6 shows a typical flow field of the hypersonic lifting-body without aerospike.

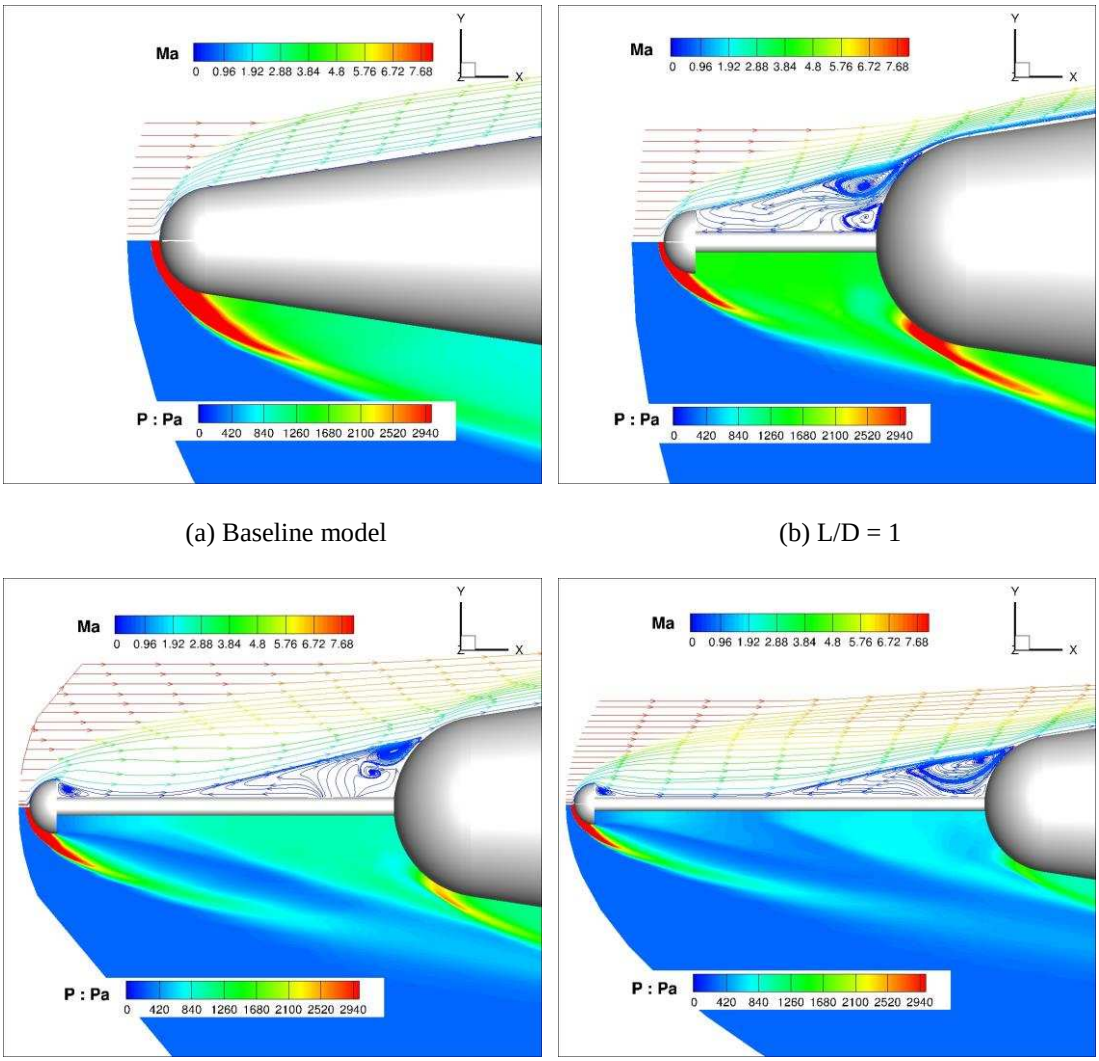

(a) Baseline model (b) L/D = 1

(c) L/D =2 (d) L/D = 3

Fig. 7 Flow field over spiked lifting-body.

In Fig. 7, it is noted that there are two flow separations which are created by the aerospike because there are two regions of adverse pressure gradient along with the aerospike. One separation appears just behind the disk of aerospike and the other separation is attached to the nose of the lifting-body. By means of the latter separation, the bow shock of vehicle nose is altered upstream, lowering down the pressure in front of the nose, causing the reduction of the pressure drag and the heat load of the nose. Moreover, on the nose of vehicle, there is a reattachment point which is forced up and downstream when L/D increases.

In order to explain the drag reduction caused by the aerospike, two methods are suggested. One

method is explicitly using “effective body” to refer to the shape of the shear layer by Yamauchi et al. [29], and the other one is using dividing streamline rather than the whole shear layer to identify the effective body by Ahmed and Qin [30]. An interesting phenomenon is that all streamlines above the dividing streamline pass downstream the body shoulder, while at the same time all streamlines below the dividing streamline reverse into the recirculation zone. Based on the works of Ahmed and Qin [30], a key fact is the angle of reattachment point θ which is measured in the counterclockwise direction from the center line of the nose to the dividing streamline on the bottom wall of nose. In Fig. 8, it is interesting to note that when L/D increases at α=0º, θ increases as well, which means the “effective body” becomes larger when the spike length increases, resulting in reduction of the nose’s pressure. Moreover, Ahmed and Qin discovered that the shape and size of the recirculation zone determines the amount of drag reduction.

Most of the previous effort was directed at α=0º, but at α=8º, the trend of θ is different, i.e. θ decreases when L/D increases. Because the flow is not symmetric in y-direction and the separation region does not always become larger in the windward side when L/D increases. Thus, a more complex method should be employed to consider the effects on both windward and leeward sides.

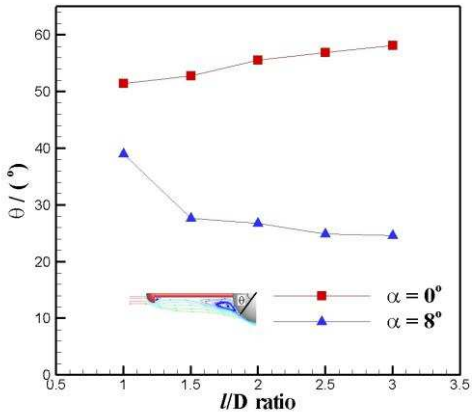

Fig. 8 Angle of reattachment point vary with L/D ratios.

Comparing the pressure distribution between α=0º and α=8º in the symmetric plane along the wall of vehicle nose in the windward side, both have the same trend that is the pressure firstly increases then decreases, showing in Fig. 9. However, at α=0º, the pressure of the case with aerospike is always lower than the pressure of the case without aerospike, meanwhile, at α=8º, the pressure of the case with aerospike can be higher than the pressure of the case without aerospike. Considering this difference discussed above, it proves that the analysis method should be developed due to the complex of flow field at an angle of attack which is not equal to zero.

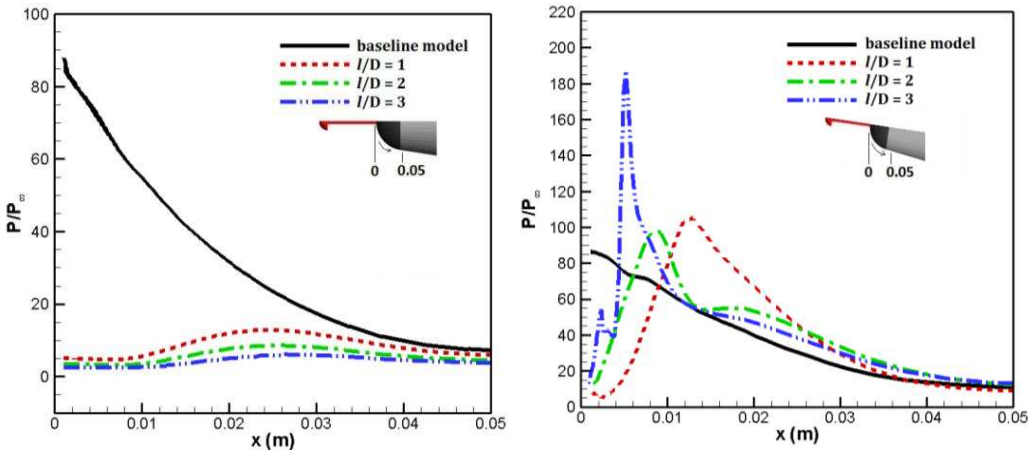

(a) α=0º (b) α=8º

Fig. 9 Pressure distribution in the symmetric plane along the wall of vehicle nose.

In the previous research, the pressure drag coefficients of vehicle nose always decrease when L/D increases, which means the aerospike should be designed as long as possible to achieve a high drag reduction with α=0º. However, looking at Fig. 10, there is an optimal point when L/D = 2.0 with α=8º, which is an important phenomenon that should be noticed during the design process of the vehicles. Because most vehicles fly at an angle of attack which is not zero when they are at gliding phase, a best L/D should be found when the aerospike is applied for the vehicle. In this case, L/D=2 is the best point, which gives 49.3% and 4.39% drag reductions for the nose part and the whole vehicle, respectively. Based on the results, the case of L/D=2 will be further analyzed by comparing the effects of different

aerospike disks to optimize the disk shape in the next subsection.

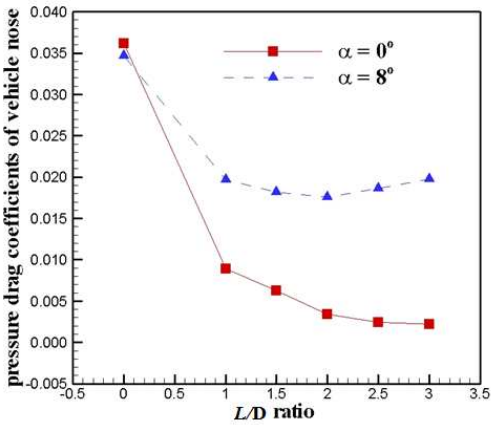

Fig. 10 Pressure drag coefficients of vehicle nose varies with L/D ratio of spike.

3.2 Effects of disk shape on drag

In this subsection, the aerospike length is fixed to be 200mm, which is L/D=2, according to the result of Section 3.1. The flat faced disk has a larger structural strength than hemispheric disk because of its geometric shape at the cruise angle, ensuring its durability under heavy lateral loads, also reduces elastic deformation at hypersonic speeds. [7] showed that the drag of the vehicle nose is remarkably influenced by the disk shape, and [18] suggested that the use of double-disk aerospike can favourably reduce drag, considering from the aspect, SFF and DFF with appropriate disk shape and position, shown in Fig. 2(b) and (c), are added in the research to compare with the hemispheric disk in order to carry out the disk shape selection.

The flow field is investigated in the nose region with different shapes of aerospike disks at α=8º in Fig. 11, showing that the flow separation is quite large behind the aerospikes due to the incidence. Additionally, DFF creates the largest separation among the three different aerospikes.

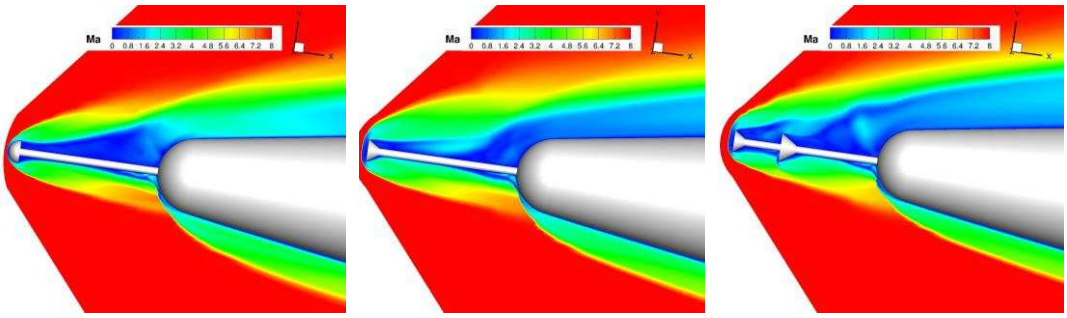

(a) Hemispheric disk aerospike (b) SFF aerospike (c) DFF aerospike

Fig. 11 Comparison of Mach number contour with different aerospikes in the nose region.

Fig. 12 shows the pressure distribution and extreme streamline on the nose of lift body, comparing DFF and SFF at the same time. The left half is DFF and the right half is SFF. From Fig. 12(a), the circle of the reattachment line from DFF is larger than the circle of the line from SFF, which means the flow separation region of the former is larger than that of the latter. Obviously, the pressure at the nose with DFF is smaller than that of the nose with SFF in four cases of different angles of attack (α=0°~ 12°), indicating that DFF is better than SFF.

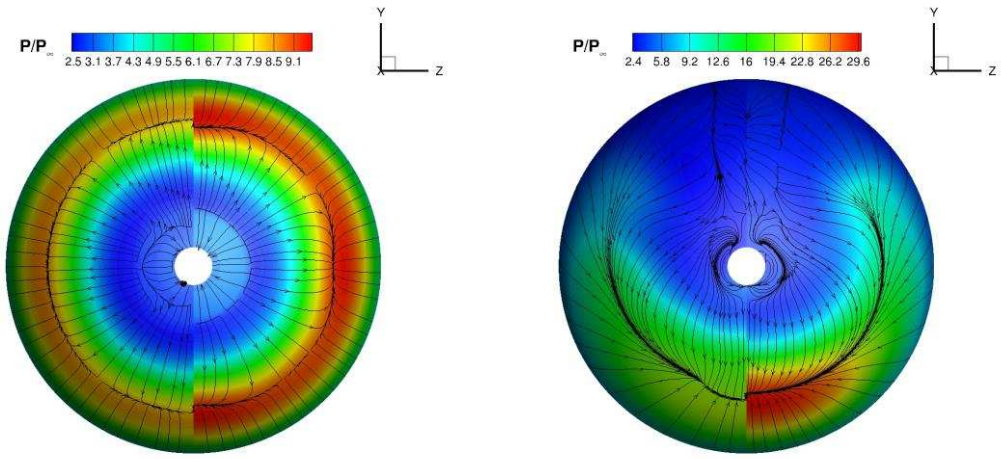

(a) α=0° (b) α=4°

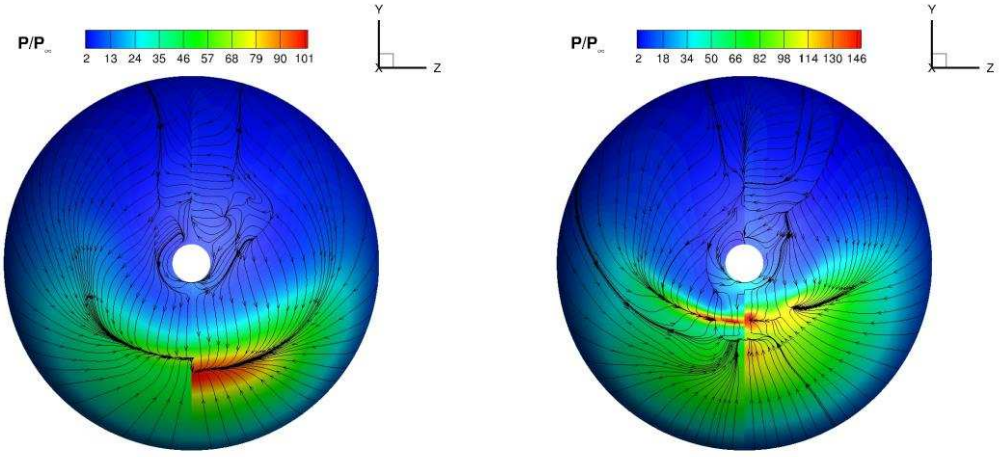

(c) α=8º (d) α=12º

Fig. 12 The pressure distribution and extreme streamline on the nose of lifting-body. The left half is with DFF and the right half is with SFF.

Table 1 shows the drag coefficients of the vehicle nose with different disk shapes and with the same L/D ratio of 2.0 at α=8º. Compared with SFF, the hemisphere disk has smaller drag on the aerospike itself and bigger drag on the nose, which shows the advantages in terms of total drag. The best disk shape is DFF which gives 60.5% drag reduction of the vehicle nose's part. The results suggest that the flow separation on the aerospike and recirculation zone formed on the nose mainly depends on the disk shape when they have the same aerospike length.

Table 1 Drag coefficients of the vehicle nose with different disks (Ma=8, α=8º)

Shape	C_D_spike	C_D_nose
Baseline model	0.0000	0.0347
Hemisphere disk	0.0032	0.0176
SFF	0.0058	0.0169
DFF	0.0068	0.0137

It can also be observed in Fig. 12 that when the angle of attack increases, the pressure value of the high-pressure region increases rapidly on the vehicle nose. For both DFF and SFF discussed above, the separation line on the bottom wall of vehicle's nose is closer to the nose center gradually when the angle of attack increases, which means the recirculation region in front of the vehicle nose of the

windward part becomes smaller gradually. According to the expression in the Subsection 3.1, the recirculation region is a key fact to judge the trend of drag reduction. Thus, when the recirculation region becomes smaller due to the increase of incidence, the drag coefficients climb up. Comparing at the same angle of attack, the pressure distribution of using DFF is lower than that of using SFF so that DFF is better than SFF to reduce drag.

Based on the preceding expression in Subsection 3.1, it is important to consider the fact that the angle of attack influences the effects of aerospike. If the installation angle of aerospike can be adapted to the flight angle in real time, the aerodynamic characteristics of the vehicle can be improved better than that of the case with a constant installation angle of aerospike. But it is very hard to be practical due to the thermal protection system and the aerospike structural strength in hypersonic. Considering the simplification and reliability of the drag reduction system, on the basis of Schulein's self-aligning aerospike [31], a double flat faced disk aerospike with an installation angle of 8º (DFFA) is employed to enhance the drag reduction effect in the next subsection.

3.3 Effects of installation angle on drag

As mentioned in the first section, Menezes [9] experimentally found that the effect of drag reduction could be significantly decreased with a non-zero angle of attack, or even worse, the aerospike could be a device inducing more drag and the heat flux. This problem can be solved by installing the aerospike with an installation angle to reduce the angle between aerospike and the incoming flow.

Comparing the flow field between DFF and DFFA, Fig. 13 shows the streamlines on symmetric plane and the pressure distribution on the wall. From Fig. 13(a) and (b), at α=0º, the separation is symmetric around the vehicle nose with DFF, but with DFFA, the separation is smaller around the top part of the vehicle nose than that around the bottom part of the vehicle. Moreover, the pressure

distribution shows that the pressure on the vehicle nose with DFFA is higher than that with DFF.

Comparing Fig.13(e) and (f), the separation is smaller around the bottom part of the vehicle nose than that around the top part of the vehicle with DFF. But note that the separation is almost symmetric around the vehicle nose with DFFA, which is a good phenomenon for DFFA, having large separation area and low pressure distribution on the wall of nose. At α=12º, DFFA is obviously better than DFF, indicating that the separation of DFFA is larger than that of DFF and the pressure of DFFA on the wall is lower than that of DFF in Fig. 13(g) and (h).

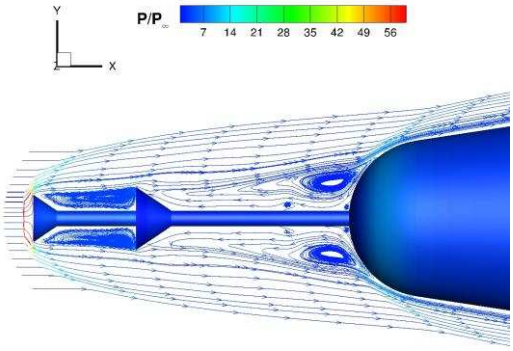

(a) $\alpha_s = 0^o, \alpha = 0^o$

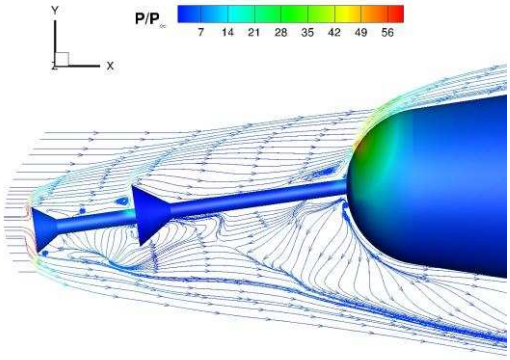

(b) $\alpha_s = 8^o, \alpha = 0^o$

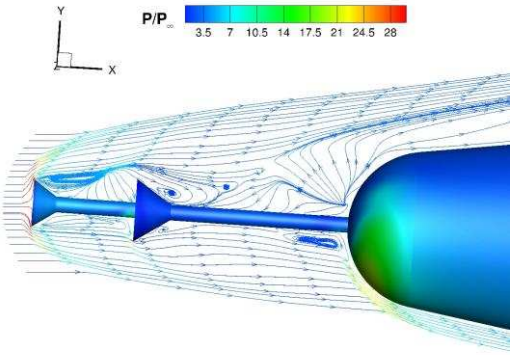

(c) $\alpha_s = 0^o, \alpha = 4^o$

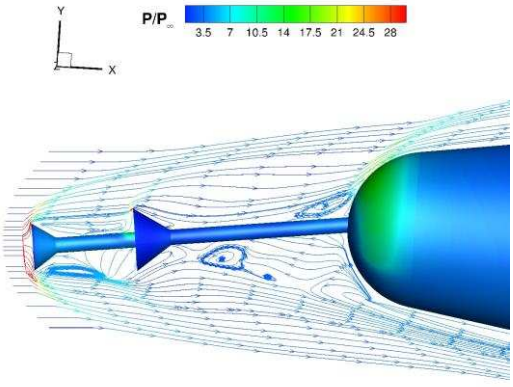

(d) $\alpha_s = 8^o, \alpha = 4^o$

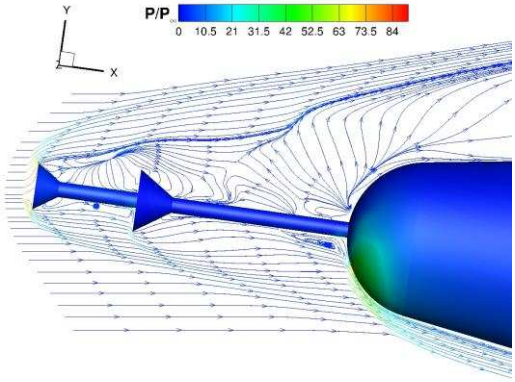

(e) $\alpha_s = 0^o, \alpha = 8^o$

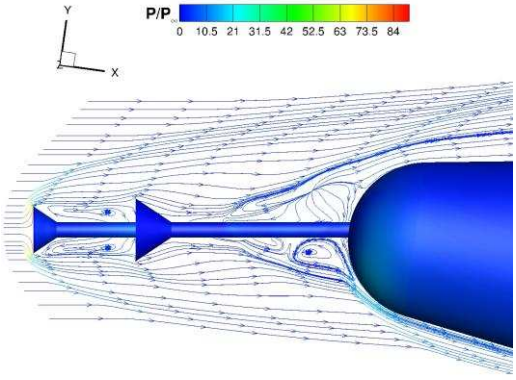

(f) $\alpha_s = 8^o, \alpha = 8^o$

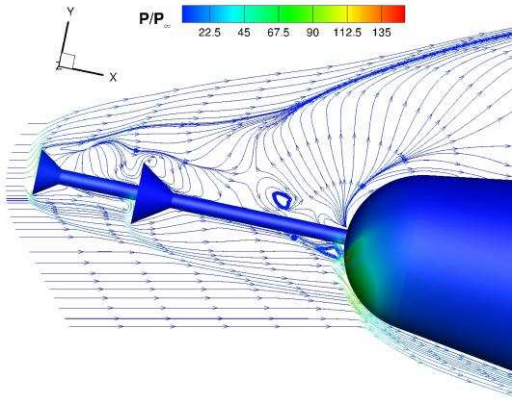

(g) $\alpha_s = 0^o, \alpha = 12^o$

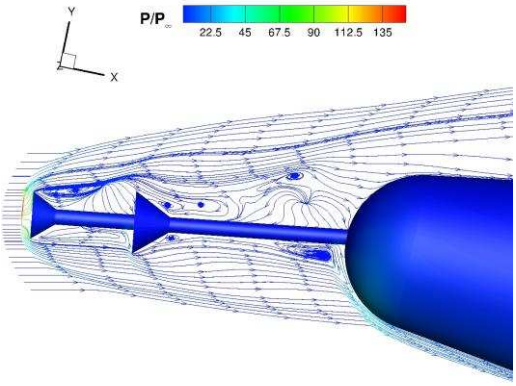

(h) $\alpha_s = 8^o, \alpha = 12^o$

Fig. 13 The streamline on symmetric surface and pressure on the wall for different angles of attack.

With an installation angle of the aerospike, the angle of attack of local flow around vehicle nose is modified, with changed pressure distribution. Fig. 14 shows that the DFF drag coefficient of vehicle nose increases nearly linearly with the angle of attack. But the DFFA drag coefficients around angle of attack 4°~10° are near constant and are relatively much lower compared with DFF drag as the incidences beyond 4°.

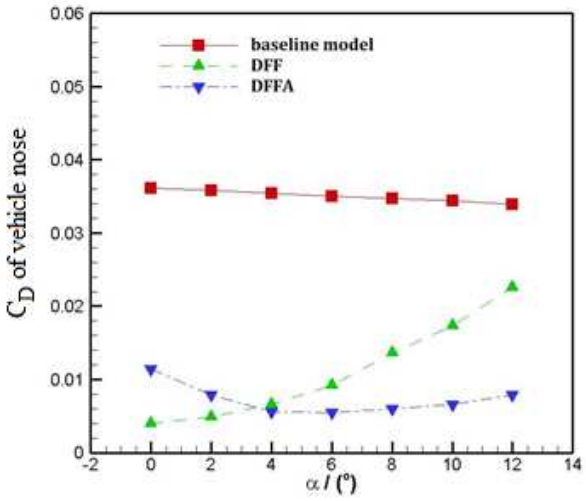

Fig. 14 Drag coefficients of the nose vary with angle of attack.

The Mach number contour on the symmetry plane is shown in Fig. 15 at α=8º to compare the baseline model and DFFA. It shows that the shock shape in the front of the nose is changed from a strong bow shack into a weak oblique shock in the case of DFFA. That is a reason why using DFFA can reduce the drag of vehicles which has been discussed in Subsection 3.1.

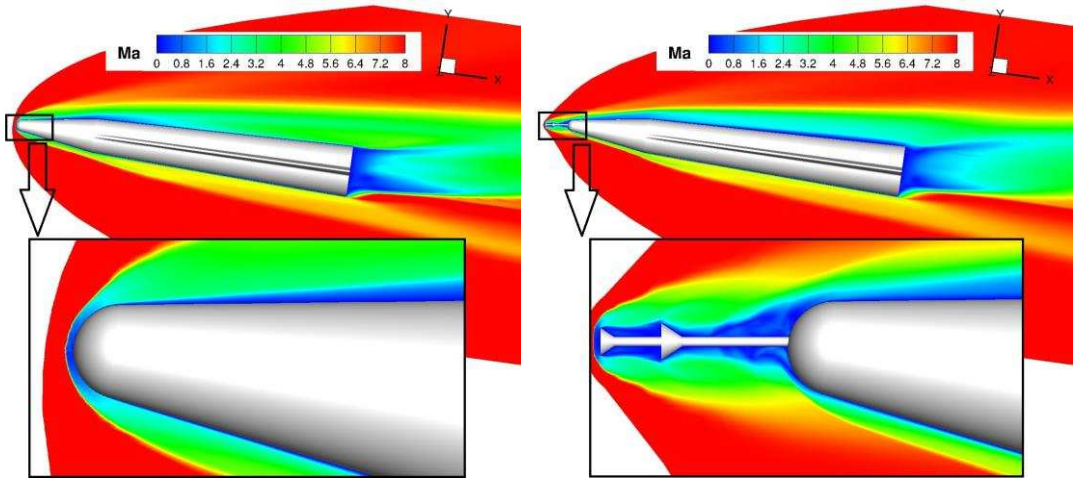

(a) Baseline model (b) Vehicle with aerospike

Fig. 15 Mach number distribution of the vehicle symmetry plane (Ma=8, α=8º).

To show the advantages of vehicles with an aerospike installed at 8º, the aerodynamic characteristics are compared in Fig. 16, including the baseline model, DFF and DFFA. From Fig. 16(a), DFF has the smallest drag at α=0º, but the drag at α=12º is almost the same as that obtained by the baseline model.

Meanwhile, the DFFA aerospike always produces less drag than the baseline model and obtains less drag than DFF at α=8º. It means the DFFA aerospike can produce a relatively steady drag-reduction and it is better to use DFFA if the vehicle is flying at a non-zero angle of attack. Fig. 16(b) shows that the aerospikes have little influence on the lift. Showing in Fig. 16(c), both DFF and DFFA aerospikes effectively improve the lift-to-drag ratio. At the same time, DFFA aerospike can both maintain the large improvement at high angles of attack and gain a better lift-to-drag ratio than the baseline model between 2°~12°, having the largest lift-to-drag ratio at α=6º. The influence on pressure center is considered insignificant and, therefore, there is almost no effect on the vertical static-stability of the vehicle, as shown in Fig. 16(d).

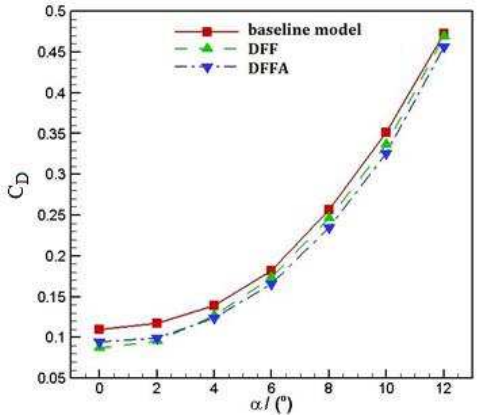

(a) Drag coefficients

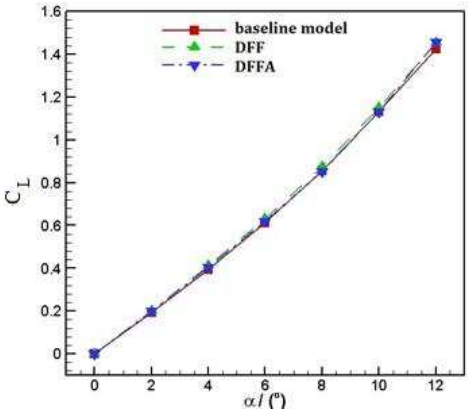

(b) Lift coefficients

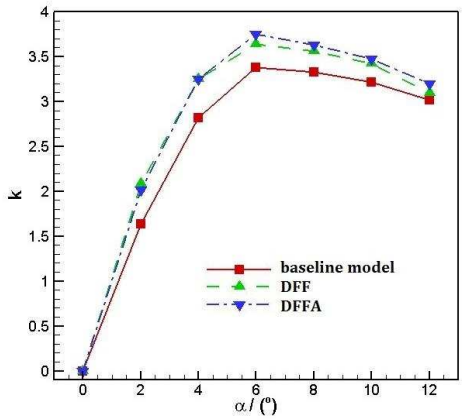

(c) Lift-to-drag ratios

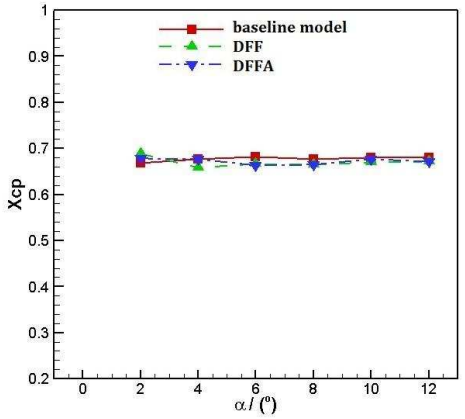

(d) Pressure center coefficients

Fig. 16 Comparison of aerodynamic characters for baseline model, double flat faced aerospike with and without installation angle at Ma = 8, α = 8º.

The effects of aerospike on vehicle lift-drag characteristics are shown in Table 2 which displays the total drag reductions due to the aerospikes. The results suggest that, by using DFF and DFFA, the lift-to-drag ratio is effectively improved around the flight angle of attack. DFFA can suppress the increase of drag at high angles of attack and enhance the lift-to-drag ratio. At α=8º, DFFA is the best choice because it produces 8.7% drag reduction and improves the lift-to-drag ratio to 3.634 which is 9.1% higher than the baseline model.

Table2 Maximum effects of aerospike on vehicle lift-drag characteristics (Ma=8, α=8º)

Shape	$\alpha = 0°$		$\alpha = 8°$							
	C_D	Effect	C_D	Effect	C_L	Effect	k	Effect	Xcp	Effect
Baseline model	0.1097	0.0%	0.2568	0.0%	0.8549	0.0%	3.329	0.0%	0.6766	0.0%
DFF	0.0870	-20.7%	0.2461	-4.2%	0.8752	2.4%	3.556	6.8%	0.6649	-1.7%
DFFA	0.0942	-14.2%	0.2346	-8.7%	0.8523	-0.3%	3.634	9.1%	0.6656	-1.6%

Comparing with the baseline model, the pressure center of the vehicle with an aerospike moves slightly forward by 1.6% and with little effect on the static stability. In general, since the incidence is 8º in the gliding phase, to obtain the best aerodynamics performance at this incidence, the most optimized aerospike is DFFA which has the drag reductions of 82.8% and 8.7% for nose and whole vehicle, respectively.

IV. Conclusions

This paper has investigated the performance of disk spikes in the context of hypersonic lifting body aerodynamics at a range of incidences. Hypersonic flow over a spiked lifting-body at Mach number 8 with different L/D ratios and disk shapes at flying angles of attack are numerically simulated. The major findings are as follows:

(1) The area of low pressure region depends on the aerospike length to nose diameter ratio which is

the main factor for drag reduction. A significant drag reduction with the application of hemispheric disk aerospike at the nose can be achieved. An aerospike with L/D = 2 gives best reduction when comparing with other L/D ratios at α=8º, which leads to a maximum drag reduction of 49.3% and 4.39% for nose and a whole vehicle, respectively.

(2) Comparison of hemispheric, single flat faced and double flat faced disks were made. The low pressure region at nose with double flat faced aerospike is larger than that with single flat faced aerospike at different angles of attack. For the vehicle nose, drag reduction caused by double flat faced aerospike is the best, having 60.5% pressure drag reduction of nose's part at flight α=8º.

(3) By installing the aerospike with a proper angle, the drag can be effectively reduced at the cruise angle. When the angle of attack is changed around the cruise angle, the drag remains at the similar value. This phenomena means the drag reduction is stable and efficient using an aerospike with an installation angle at the gliding phase. The drag reduction of the whole vehicle is 8.7% at α=8º, using double flat faced aerospike. The lift-to-drag ratio is 3.634, which is 9.1% better than the baseline model.

Acknowledgments

The authors would like to thank China Scholarship Council (CSC) and the Aerospace International Innovation Talent Cultivation Project (AIITCP) Program for their support. This work was funded by CSC and finished with researchers of University of Sheffield as an academic visitor.

References

[1] Kremeyer, K., Reilly, M. P., and Miley, G. H., "Lines of Energy Deposition for Supersonic/hypersonic Temperature/drag-reduction and Vehicle Control,"AFRL-RZ-ED-TP-2009-359, 2009.

[2] Sun, X., Guo, Z., Huang, W., Li, S. B., and Yan, L., "Drag and Heat Reduction Mechanism Induced by a Combinational Novel Cavity and Counterflowing Jet Concept in Hypersonic Flows,"Acta Astronautica, 2016, 126: 109-119.

[3] Wang, Z., Sun, X., Huang, W., Li, S. B., and Yan, L., "Experimental Investigation on Drag and Heat Flux Reduction in Supersonic/Hypersonic Flows: A survey," Acta Astronautica, 2016, 129: 95-110.

[4] Jiang, Z., Liu, Y., Han, G., and Zhao, W., "Experimental demonstration of a new concept of drag reduction and thermal protection for hypersonic vehicles," Acta Mechanica Sinica, 2009, 25(3): 417-419.

[5] Crawford, D., "Investigation of the Flow over a Spiked-nose Hemisphere-cylinder," NASA TN-D-118,1959.

[6] Motoyama, N., Mihara, K., Miyajima, R., Watanuki, T., and Kubota, H., "Thermal Protection and Drag Reduction with use of Spike in Hypersonic Flow," AIAA 2001-1828, 2001.

[7] Mehta, R. C., "Flow Field Computations over Conical, Disc and Flat Spiked Body at Mach 6,"AIAA 2009-325, 2009.

[8] Menezes, V., Saravanan, S., Reddy, K. P. J., "Shock Tunnel Study of Spiked Aerodynamic Bodies Flying at Hypersonic Mach Numbers," Shock Waves, 2002, 12(3): 197-204.

[9] Menezes, V., Saravanan, S., Jagadeesh, G., and Reddy, K. P. J., "Experimental Investigations of Hypersonic Flow over Highly Blunted Cones with Aerospikes," AIAA journal, 2003, 41(10): 1955-1966.

[10] Kulkarni, V., Kulkarni P, S., and Reddy, K. P. J., "Drag Reduction by a Forward Facing Aerospike for a Large Angle Blunt Cone in High Enthalpy Flows," Shock Waves, Springer Berlin Heidelberg, 2009: 565-570.

[11] Gauer, M., and Paull, A., "Numerical Investigation of a Spiked Blunt Nose Cone at Hypersonic Speeds," Journal of Spacecraft and Rockets, 2008, 45(3): 459-471.

[12] Boylan, D. E., Hahn, J. S., and Sims, W. H., "Drag on Blunt Bodies with and without Spikes in Low-density Hypersonic Flow," AIAA Journal, 1965, 3(2): 365-366.

[13] Kalimuthu, R., Mehta, R. C., and Rathakrishnan, E., “Experimental Investigation on Spiked Body in Hypersonic Flow,” Aeronautical Journal, 2008, 112(1136): 593-598.

[14] Asif, M., Zahir, S., Kamran, N., and Khan, M. A., “Computational Investigations Aerodynamic Forces at Supersonic/hypersonic Flow past a Blunt Body with Various Forward Facing Spikes,” AIAA 2004-5189, 2004.

[15] Gerdroodbary, M. B., and Hosseinalipour, S. M., “Numerical Simulation of Hypersonic Flow over Highly Blunted Cones with Spike,” Acta Astronautica, 2010, 67(1): 180-193.

[16] Elsamanoudy, M., Ghorab, A., and Hendy, M., “Drag Reduction using Spiked-aerodisk & Reattachment Ring for Hypersonic Hemispherical Bodies,”15th International Conference on Aerospace Sciences&Aviation Technology, ASAT-15-151-AE, 2013.

[17] Tahani, M., Karimi, M. S., Motlagh, A. M., and Mirmahdian, S., “Numerical Investigation of Drag and Heat Reduction in Hypersonic Spiked Blunt Bodies,” Heat and Mass Transfer, 2013, 49(10): 1369-1384.

[18] Yadav, R., and Guven, U., “Aerothermodynamics of a Hypersonic Projectile with a Double-disk Aerospike,” Aeronautical Journal, 2013, 117(1195): 913-928.

[19] Joshi, S., “Effect of Double Disk Aero-spikes on Aerothermodynamics of Blunt Body at Mach 6.2,” International Journal of Applied Engineering Research, 2016, 11(1): 366-376.

[20] Ahmed, M. Y. M., and Qin, N., “Surrogate-based Multi-objective Aerothermodynamic Design Optimization of Hypersonic Spiked Bodies,” AIAA journal, 2012, 50(4): 797-810.

[21] Ahmed, M. Y. M., and Qin, N., “Recent Advances in the Aerothermodynamics of Spiked Hypersonic Vehicles,” Progress in Aerospace Sciences, 2011, 47(6): 425-449.

[22] Srulijes, J., Gnemmi, P., Runne, K., and Seiler, H., “High-pressure Shock Tunnel Experiments and CFD Calculations on Spike-tipped Blunt Bodies,” AIAA Journal, 2002, 5(1):2918-2926.

[23] Schulein, E., "Wave Drag Reduction Approach for Blunt Bodies at High Angles of Attack: Proof-of-concept Experiments," AIAA 2008-4000, 2008.

[24] Schülein, E., "Wave Drag Reduction Concept for Blunt Bodies at High Angles of Attack," Shock Waves, 2009, 4(1):1315-1320.

[25] McWherter, S. C., Moua, C. M., Gera, J., and Cox, T. H., "Stability and Control Analysis of the F-15B Quiet Spike™ Aircraft," NASA/TM-2009-214651, 2009.

[26] Khurana, S., and Suzuki, K., "Aerothermodynamics of Lifting-body Configuration in Hypersonic Flow with Aerodisk at Nose," AIAA 2014-1247, 2014.

[27] Kimmel, R., Adamczak, D., Juliano, T, and Paull, A., "HIFiRE-5 Flight Test Preliminary Results," AIAA 2013-0377, 2013.

[28] Kimmel, R. L., Adamczak, D., Borg, M., Juliano, T., and Stanfield, S., "HIFiRE-1 and HIFiRE-5 Test Results," AFRL-RQ-WP-TR-2014-0038, 2014.

[29] Yamauchi, M., Fujii, K., and Higashino, F., "Numerical Investigation of Supersonic Flows around a Spiked Blunt Body," Journal of Spacecraft and Rockets,1995,32(1):32-42.

[30] Ahmed, M., and Qin, N., "Drag Reduction using Aerodisks for Hypersonic Hemispherical Bodies," Journal of Spacecraft and Rockets, 2010, 47(1): 62-80.

[31] Schnepf, C., Wysocki, O., and Schülein, E. , "Wave Drag Reduction due to a Self-aligning Aerodisk," Progress in Flight Physics, 2015, 7: 475-488.